Archive of Applied Mechanics (2025) 95:155
https://doi.org/10.1007/s00419-025-02868-7

ORIGINAL

Emilija Jočić · Marija Todorović · Ivan Glišović · Miroslav Marjanović

An efficient computational model for progressive failure analysis of cross-laminated timber panels

Received: 8 July 2024 / Accepted: 5 June 2025

Abstract The paper introduces an efficient model for progressive failure analysis of cross-laminated timber panels under out-of-plane bending load. To provide the computational efficiency, the model kinematics is based on the full-layerwise plate theory of composite materials, providing 3D stress and strain fields necessary for accurate prediction of damage initiation and progression. Damage initiation and associated failure mode on the lamina level are determined using the 3D Hashin failure criterion, while the post-failure behaviour is described using a smeared crack band model introducing the bilinear strain-softening curves. The model allows capturing different timber response in tension (brittle) and compression (ideally plastic) in the entire considered (3D) domain. The computational analyses are performed using an original layered finite element framework, while the model validation is done through the extensive experimental testing programme on full-scale CLT specimens. Excellent agreement of obtained load–deflection curves and strain distributions verified that the proposed methodology can be efficiently applied in progressive failure analysis of mass timber, but also in other layered beam- and plate-like structures in bending.

Keywords Progressive failure analysis · Cross-laminated timber · Out-of-plane bending · Layered finite elements · Layerwise theory

1 Introduction

Cross-laminated timber (CLT) is a massive wood composite made by glueing crosswise layers (laminas) of solid timber boards to form large-scale panels. Due to their outstanding strength, dimensional stability, aesthetic quality and fire resistance, CLT panels have been widely used in structural engineering during the last decade. A low-carbon footprint of CLT encourages its use in contemporary residential and commercial buildings instead of conventional mineral-based materials [1, 2]. In the early 2000s, the use of CLT in building construction increased significantly due to the green building policy [3]. The ease of prefabrication and short erection time on site allows for CLT to be used in mid- and high-rise buildings, while a low self-weight reduces the required size of foundations and provides the potential of CLT in seismically active areas. The crosswise orientation of layers ensures uniform shrinkage and swelling properties, with high energy efficiency and capacity for storing moisture and thermal energy [4, 5].

A crosswise lay-up of the highly anisotropic timber layers causes unpredictable and unconventional failure mechanisms of CLT panels in bending. As expected, the dominant failure mode in bending is a brittle tensile failure in the bottom longitudinal layers [6, 7]. However, as suggested by Nie [8], a variation of annual ring pattern in the orthogonal (cross) timber layers causes low transverse shear strength of the cross layers and thus results in the rolling shear brittle failure [9]. This scenario is also observed by Sciomenta et al. [10],

E. Jočić · M. Todorović · I. Glišović · M. Marjanović (✉)
Faculty of Civil Engineering, University of Belgrade, Bulevar Kralja Aleksandra 73, 11000 Belgrade, Serbia
e-mail: mmarjanovic@grf.bg.ac.rs

Published online: 24 June 2025

who performed four-points bending tests on two series of three-layered CLT panels, accompanied with the analytical solution for panels in bending. Mestek et al. investigated a design concept for CLT reinforced with self-tapping screws to improve its resistance to shear failure at the supports [11], while Zhou et al. [12] also pointed out that CLT panels with low span-to-depth ratios suffer from rolling shear failure.

In all mentioned investigations, the failure estimation is generally limited to a global behaviour, without analysing the damage progression in various failure modes. However, understanding the failure modes and damage evolution within the CLT is highly important. For this reason, a detailed evaluation of CLT plate-bending tests was performed by Hochreiner et al. [13, 14]. The global load–displacement behaviour and the observed failure modes were experimentally obtained and discussed. Franzoni et al. investigated the bending behaviour of CLT panels [6] using the linear elastic exact 3D solution of Pagano [15, 16] for global analysis and van der Put failure criterion [17] for failure analysis. The assessment of cross-laminated timber panels by the state-space approach has been done by Albostami et al. [18], while Navaratnam et al. used the digital image correlation for identifying failure characteristics of CLT under transverse loading [19].

Besides prediction of the failure onset in CLT, a post-failure behaviour of CLT panels under combined out-of-plane bending and compression loads [20] was also the thematic of comprehensive investigation. The post-failure behaviour can be predicted by treating the cross layers as mechanical joints that connect the longitudinal layers [21–23]. However, the material stiffness depends on the joint efficiency of the cross layers, which is theoretically determined by the cross layer shear properties and the bonding degree. These cannot be quantitatively evaluated due to the complexity of the shear damage mode [24], and thus the current design codes employ effective bending stiffness to account for the stiffness degradation (i.e. Gamma method, shear analogy method, etc.) [25].

A post-failure behaviour prediction of CLT requires refined computational models to support the experimental studies and allow for efficient parametric analysis. Qui et al. developed XFEM based models to simulate the crack propagation behaviour of wood [26], while Yunxiang et al. [27] investigated the feasibility of CLT panels by evaluating the flexural and shear properties through mechanical tests and extensive computational analysis. For detailed description of damage evolution in CLT, distinguishing among different failure modes, the smeared crack band (SCB) approach can be used. It is originally developed by Williams et al. for the macroscopic sub-laminate level modelling of conventional composites [28] and further improved in [29–33] to account for realistic damage prediction in preferred material orientation and minimize the mesh dependency problem. Although these improvements resulted in a good compromise between computational cost and solution accuracy, the application of SCB approach in CLT is relatively rare with only few examples given in the book of Ibrahimbegović [34] and work of Lavrenčič and Brank [35]. The limited application of SCB in the analysis of CLT mostly originates from the fact that the SCB is usually coupled with the finite element methods based on the solid (brick) elements, which leads to the computationally expensive simulations due to high number of elements used for modelling the layered nature of CLT.

This paper aims to change this situation, by proposing the reliable and efficient SCB-based prediction model for progressive failure analysis of CLT panels under out-of-plane bending. The model bypasses the use of solid finite elements, by employing the layerwise kinematics based on the Reddy's full-layerwise plate theory of composite materials [36]. The model kinematics provides the 3D stress and strain field on the lamina level, necessary for accurate prediction of damage initiation and progression. Damage initiation and failure modes on the lamina level are determined using the 3D Hashin failure criterion [37] with typical strength values of timber material. The post-failure behaviour of timber is described by distinct bilinear strain-softening curves to capture timber response in tension (brittle) and compression (ideally plastic), using the SCB approach. The entire computation is performed through the original layered finite element framework [38, 39], which is extended within this research to account for the post-failure behaviour of CLT. Finally, the model validation is done through the extensive experimental testing programme on full-scale CLT specimens, and excellent agreement is obtained. Therefore, the proposed methodology can be efficiently applied in progressive failure analysis of mass timber and other layered beam- and plate-like structures, contributing to the emerging field of computational mechanics of bio-based composite structures.

2 Smeared crack band (SCB) damage model for cross-laminated timber

From the mechanics point of view, timber is an orthotropic material with three principal material axes (Fig. 1, left). Accordingly, six possible principal crack propagation directions may be identified as shown in Fig. 1, right, where the first index denotes the normal to the crack surface and the second index denotes the direction of crack propagation.

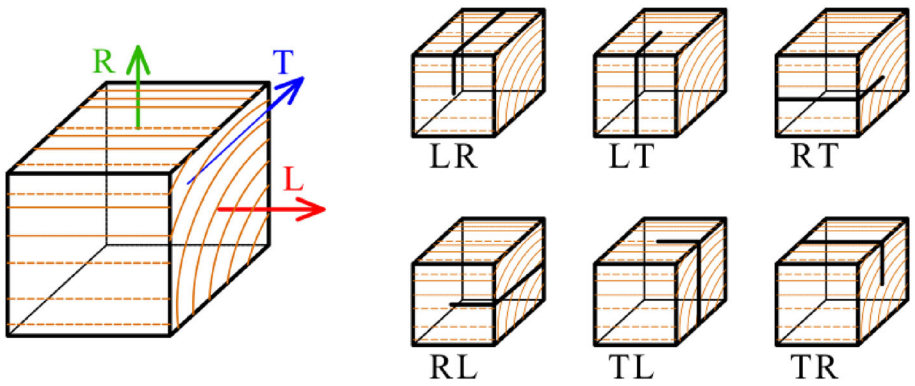

Fig. 1 Principal material directions for timber (left): L—wood fibre direction, R—radial, T—tangential; crack propagation directions (right)

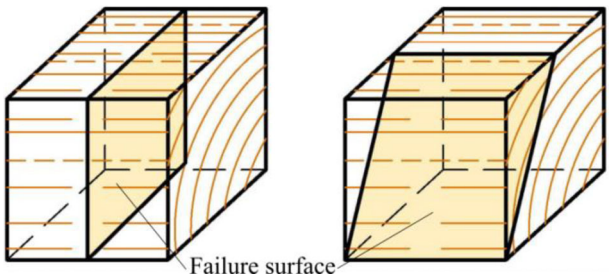

Fig. 2 Typical failure surface for: fibre tension (FT) failure mode (left); rolling shear (RS), failure mode (right)

The crosswise lay-up of the highly anisotropic timber layers yields relatively complex failure behaviour of CLT in bending. Each CLT layer is made of timber boards placed side by side with different growth rings' orientation, leading to an unknown orientation of the material coordinate system. Therefore, a homogenization on the lamina level is done by introducing the unique material coordinate system (123) established for each layer, where direction 1 aligns with longitudinal direction (parallel to grain), while directions 2 and 3 represent radial and tangential directions, respectively. To overcome the growth rings irregularity and simplify the modelling, the same material properties are assumed for directions 2 and 3 and thus the homogenization of growth rings' orientation is achieved, which is a common practice in structural analysis of CLT.

2.1 Damage model development

2.1.1 Damage initiation and failure modes for timber

The damage initiation and failure modes for timber are determined by applying the 3D Hashin failure criterion [37] considering typical strength values of timber material, considering four failure modes:

- *Fibre tension* failure (**FT**) — the most dominant and critical failure mode occurring due the tensile stress parallel to the wood fibre. This mode is characterized by the failure surface that propagates perpendicular to the wood fibre (Fig. 2, left).
- *Transverse tension* failure (**TT**), which arises due to the combined in-plane shear stress and tensile or shear stress perpendicular to the wood fibre. The failure surface is usually in the interior of the transverse lamina, following as long as possible the annual rings. This failure mode is mostly denoted as a rolling shear failure (RS) — see Fig. 2, right.
- *Fibre compression* failure (**FC**), which leads to the typical fibre kinking band formation, due to the local instabilities of the wood cells. This phenomenon results in a quasi-plastic behaviour on the macro scale.
- *Transverse compression* failure (**TC**) generally results from shear stress and compressive stresses perpendicular to the wood fibre, where the corresponding failure surface is usually parallel to the wood fibre.

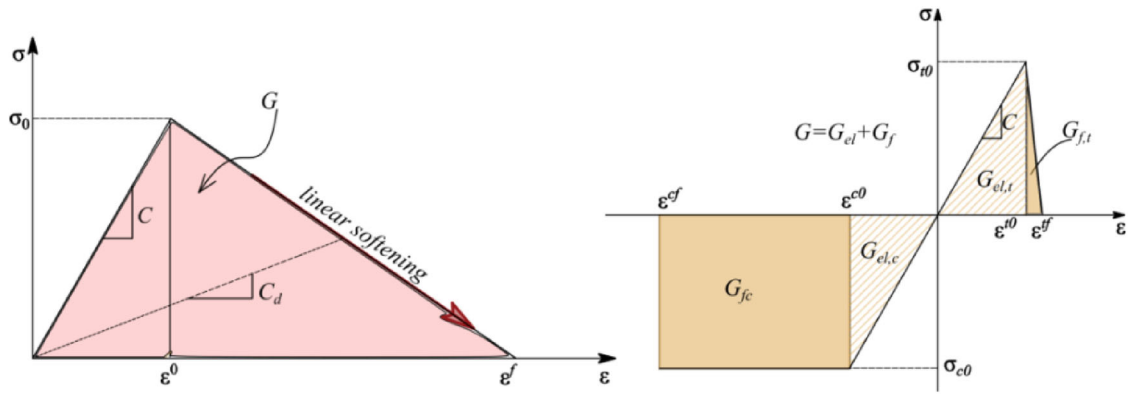

Fig. 3 General constitutive relationship with linear softening law applied in smeared crack band damage model (left); improved constitutive relationship for timber with modified softening laws (right)

The above failure modes for timber are described within a Hashin criterion as:

$$FT = \left(\frac{\sigma_1}{f_t}\right)^2 + \left(\frac{\tau_{12}}{f_v}\right)^2 + \left(\frac{\tau_{13}}{f_v}\right)^2 \geq 1, \qquad \sigma_1 \geq 0 \tag{1a}$$

$$FC = \left(-\frac{\sigma_1}{f_c}\right)^2 \geq 1, \qquad \sigma_1 \leq 0 \tag{1b}$$

$$TT = \left(\frac{\sigma_2 + \sigma_3}{f_{t,90}}\right)^2 + \left(\frac{\tau_{12}}{f_v}\right)^2 + \left(\frac{\tau_{13}}{f_v}\right)^2 + \frac{\tau_{23}^2 - \sigma_2\sigma_3}{f_{v,TR}^2} \geq 1, \qquad \sigma_2 + \sigma_3 \geq 0 \tag{1c}$$

$$\begin{aligned} TC = {} & \frac{1}{f_{c,90}}\left(\left(\frac{Y_c}{2f_{v,RT}}\right)^2 - 1\right)(\sigma_2 + \sigma_3) + \frac{1}{4f_{v,RT}^2}(\sigma_2 + \sigma_3)^2 + \\ & + \frac{1}{f_{v,RT}^2}\left(\tau_{23}^2 - \sigma_2\sigma_3\right)^2 + \left(\frac{\tau_{12}}{f_v}\right)^2 + \left(\frac{\tau_{13}}{f_v}\right)^2 \geq 1, \qquad \sigma_2 + \sigma_3 \leq 0 \end{aligned} \tag{1d}$$

In previous equations, σ_i and τ_{ij} are normal and shear stresses in material coordinate system (on the lamina level), f_t is tensile strength of timber in the longitudinal direction, f_v is longitudinal shear strength, f_c is compressive strength in the longitudinal direction, $f_{t,90}$ is tensile strength in the transverse direction to the wood fibres, $f_{c,90}$ is compressive strength in the transverse direction, and $f_{v,RT}$ is transverse shear strength. The FT and RS failure modes can be related to the LT-LR and TL-RL crack propagation scenarios (see Fig. 1), respectively. Compression failure modes (FC and TC) are not of significant importance for timber in bending, since cracks have more considerable impact on the failure behaviour when compared to the compression damage.

2.1.2 Damage evolution

Once the failure has been initiated, the damaged domain must be unloaded in a proper manner, so the stresses can be redistributed to the remaining undamaged material. As damage progresses, the analysis is performed through the material stiffness degradation controlled by damage variables. For each failure mode, these variables are defined such that they have values between zero (undamaged status) and one (complete damaged status). The evolution of each damage variable is governed by equivalent strain ε_{eq}, thus simplifying each damage mode to a 1D stress–strain problem.

In smeared formulations, such as SCB, the fracture energy is distributed over the entire volume of the considered domain. The response of damaged lamina, in both parallel and perpendicular to the fibre direction, is described by distinct bilinear strain-softening curves (Fig. 3, left), where the peak stresses coincide with the strength parallel and perpendicular to the wood fibre, respectively.

Besides tailoring the Hashin damage criterion to be applicable for analysis of timber material, the main challenge in the presented study was to adapt the conventional SCB model to be applicable in the failure prediction of CLT structures. For this purpose, the softening curves in tension and compression are adjusted

(Fig. 3, right) to capture distinct post-failure behaviours of timber in tension (brittle) and compression (ideally plastic). The considered damage law assumes that the total released strain energy of the considered domain is equal to the energy needed to create a crack that passes through it. The released strain energy of a failed domain (i.e. finite element) is determined as a product of the area under the stress–strain curve (Fig. 3, right) and characteristic domain length (i.e. it can be adopted as a square root of a finite element area—l_c).

In the presented formulation, the released strain energy is set to be equal to the dissipated fracture energy of the timber. As illustrated in Fig. 3, right, dissipated fracture energy (G) is comprised of two components: the elastic energy at failure initiation G_{el} (striped triangles area) and the post-failure fracture energy G_f (solid area). Post-failure fracture energy G_f is a material property to be experimentally obtained, while the elastic energy can be easily obtained in the moment of damage initiation. The tensile brittle post-failure behaviour of damaged lamina was defined by setting a relatively small value for $G_{f,t}$(i.e. $G_{f,t} = 145$ J/m^2, according to [40]), while the plastic compressive response was described by a constant stress–strain relation in compression.

The equivalent strain and corresponding equivalent stress for each failure mode are defined as follows:

$$\varepsilon_{FT,eq} = \sqrt{\langle\varepsilon_1\rangle^2 + \gamma_{12}^2 + \gamma_{13}^2}, \qquad \sigma_{FT,eq} = \frac{\langle\sigma_1\rangle\langle\varepsilon_1\rangle + \tau_{12}\gamma_{12} + \tau_{13}\gamma_{13}}{\varepsilon_{FT,eq}} \tag{2a}$$

$$\varepsilon_{FC,eq} = \langle-\varepsilon_1\rangle, \qquad \sigma_{FC,eq} = \frac{\langle-\sigma_1\rangle\langle-\varepsilon_1\rangle}{\varepsilon_{FC,eq}} \tag{2b}$$

$$\begin{aligned} \varepsilon_{TT,eq} &= \sqrt{\langle\varepsilon_2\rangle^2 + \langle\varepsilon_3\rangle^2 + \gamma_{12}^2 + \gamma_{13}^2 + \gamma_{23}^2}, \\ \sigma_{TT,eq} &= \frac{\langle\sigma_2\rangle\langle\varepsilon_2\rangle + \langle\sigma_3\rangle\langle\varepsilon_3\rangle + \tau_{12}\gamma_{12} + \tau_{13}\gamma_{13} + \tau_{23}\gamma_{23}}{\varepsilon_{TT,eq}} \end{aligned} \tag{2c}$$

$$\begin{aligned} \varepsilon_{TC,eq} &= \sqrt{\langle-\varepsilon_2\rangle^2 + \langle-\varepsilon_3\rangle^2 + \gamma_{12}^2 + \gamma_{13}^2 + \gamma_{23}^2}, \\ \sigma_{TC,eq} &= \frac{\langle-\sigma_2\rangle\langle-\varepsilon_2\rangle + \langle-\sigma_3\rangle\langle-\varepsilon_3\rangle + \tau_{12}\gamma_{12} + \tau_{13}\gamma_{13} + \tau_{23}\gamma_{23}}{\varepsilon_{TC,eq}} \end{aligned} \tag{2d}$$

where $\langle\ \rangle$ denotes the Macaulay bracket. Using the equivalent strain, damage variables in tension can be calculated using the following relation (J = FT or TT):

$$d_J = \frac{\varepsilon_{J,eq}^f\left(\varepsilon_{J,eq} - \varepsilon_{J,eq}^0\right)}{\varepsilon_{J,eq}\left(\varepsilon_{J,eq}^f - \varepsilon_{J,eq}^0\right)}, \qquad \varepsilon_{J,eq}^0 \le \varepsilon_{J,eq} \le \varepsilon_{J,eq}^f \tag{3}$$

where $\varepsilon_{J,eq}^0$ is the equivalent strain at the damage initiation ($d_J = 0$) and $\varepsilon_{J,eq}^f$ is the equivalent strain at the final failure ($d_J = 1$):

$$\varepsilon_{J,eq}^f = \frac{2G_J}{l_c\sigma_{J,eq}^0} \tag{4}$$

In Eq. (3), $\sigma_{J,eq}^0$ is the equivalent stress at the damage initiation, l_c is the characteristic domain length, and G_J dissipated fracture energy. Damage variables for compressive failure modes are calculated in the way to ensure the constant stress after yielding initiation (J = FC or TC):

$$d_J = \frac{\varepsilon_{J,eq} - \varepsilon_{J,eq}^0}{\varepsilon_{J,eq}}, \qquad \varepsilon_{J,eq}^0 \le \varepsilon_{J,eq} \le \varepsilon_{J,eq}^f \tag{5}$$

The damage variables d_J for the kth lamina are used to derive the 3D constitutive matrix of the damaged material $C_d^{(k)}$, and they are provided in [39].

Finally, the stresses for the k^{th} lamina in the damaged state are then evaluated as:

$$\left\{\sigma_{1,d}\ \sigma_{2,d}\ \sigma_{3,d}\ \tau_{23,d}\ \tau_{13,d}\ \tau_{12,d}\right\}^{(k)T} = \mathbf{C}_d^{(k)}\left\{\varepsilon_1\ \varepsilon_2\ \varepsilon_3\ \gamma_{23}\ \gamma_{13}\ \gamma_{12}\right\}^{(k)T} \tag{6}$$

After dividing the load in the load steps, the iterative procedure is performed in each load step and the damaged material properties are utilized within the considered load step/iteration to describe the post-failure

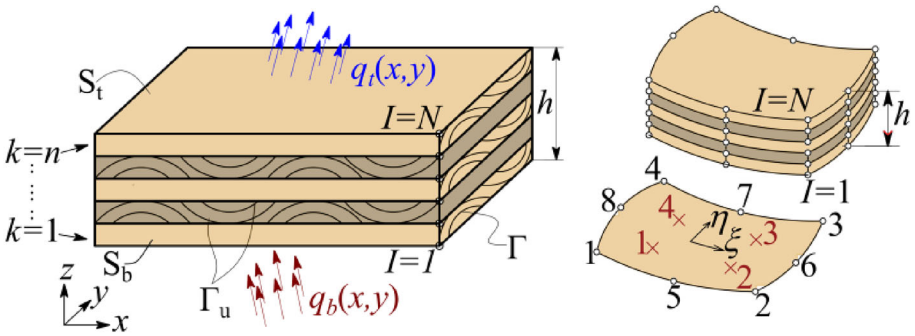

Fig. 4 Laminated composite plate made of n material layers and N numerical interfaces (left); quadratic serendipity Q8 layered element with linear layerwise thickness interpolation and corresponding reduced integration Gauss quadrature points (right)

behaviour of damaged material. The damaged material properties are updated (reduced) and then substituted into the constitutive matrix $C_d^{(k)}$. By keeping the same load in the considered load step, a new iteration is performed with the modified material properties and the process is repeated until there is no more material modifications within the considered load step (no further damage is obtained). This completes the procedure of the progressive failure analysis of the CLT using the smeared crack band model. The analysis can be used regardless of the computational method used to obtain the stress field in the considered domain.

2.2 Finite element formulation

As stated in the previous section, the progressive failure analysis (PFA) requires the accurate evaluation of 3D stress field in the considered domain, in every load step. When applied to CLT, stress evaluation should be done in every lamina, in the material (local) coordinate system. In this study, a full-layerwise (FLWT) finite element formulation of a CLT panel made of n perfectly bonded layers is considered (Fig. 4, left). The total plate thickness is denoted as h, while the thickness of the k^{th} lamina is denoted as h_k. The plate is supported along the portion Γ_u of the boundary Γ and loaded with $q_t(x,y)$ and $q_b(x,y)$ acting to either top or the bottom surface of the plate (S_t or S_b).

In the LW approach, the displacement field (u,v,w) of an arbitrary point (x,y,z) of the laminate is given as:

$$u(x,y,z)=\sum_{I=1}^{N} U^I(x,y)\Phi^I(z),\quad v(x,y,z)=\sum_{I=1}^{N} V^I(x,y)\Phi^I(z),\quad w(x,y,z)=\sum_{I=1}^{N} W^I(x,y)\Phi^I(z) \tag{7}$$

In Eq. (7), $U^\text{I}(x,y)$, $V^\text{I}(x,y)$, and $W^\text{I}(x,y)$ are the displacement components in the I^{th} numerical interface of the plate in directions x, y and z, respectively, while N is the number of interfaces between the layers including S_t and S_b. $\Phi^\text{I}(z)$ are linear layerwise continuous functions of the z-coordinate, associated with the considered interface I. Piece-wise linear variation of all three displacement components through the thickness is imposed, leading to the layerwise 3D stress field. The z-coordinate is further eliminated by the explicit integration of stresses multiplied with the corresponding functions $\Phi^\text{I}(z)$ [36].

In the finite element formulation, all displacement components are interpolated using the same 2D interpolation polynomials. Element stiffness matrix is obtained in a common way, using 2D Gauss–Legendre quadrature for quadrilateral domains. Quadratic serendipity (Q8) layered quadrilateral elements with reduced integration have been considered (Fig. 4, right). Once the nodal displacements are obtained, stresses are evaluated from the constitutive relations in the Gauss points of the considered element in every interface along the plate thickness, both in the laminate (xyz) and in the local (123) coordinate systems. Since the interlaminar stresses calculated from the constitutive equations are discontinuous at lamina interfaces, they are re-computed by assuming a quadratic distribution through each lamina, using the procedure given in [41]. The finite element model is implemented within a FLWTFEM open-source code by authors, while GUI and post-processing is performed using GiD [42].

Table 1 Material strength properties [MPa]

E_{L} (exp)	f_{t} (exp)	f_{c} (exp)	f_{v} (exp)	$f_{\mathrm{t,90}}$ [48]	$f_{\mathrm{c,90}}$ [48]	$f_{\mathrm{v,TR}}$ [48]
11242	43.8	36.3	5.3	3.0	6.0	3.0

Table 2 Material elastic properties [MPa]

E_L	E_T	E_R	G_{LT}	G_{LR}	G_{RT}	ν_{LT} (-)	ν_{LR} (-)	ν_{TR} (-)
11242	899.36	562.1	803	754.82	80.3	0.37	0.42	0.47

3 Model validation and discussion

3.1 Timber properties

To validate the modelling approach, an extensive experimental programme of CLT panels subjected to out-of-plane bending was conducted in the Laboratory of Structures at the Faculty of Civil Engineering, University of Belgrade. Preliminary tests were conducted on small clear timber samples in order to assess the quality of local timber used for the production of CLT. The strength class of timber was evaluated in accordance with EN 338 [43], based on bending strength, modulus of elasticity parallel to grain and density. It was concluded that timber used for the production of CLT panels meets the criteria for classification in the strength class C24 according to EN 338.

Four-point bending test was carried out in accordance with EN 408 [44]. A total of 20 prismatic samples with square cross Sect. 20×20 mm and length in the wood fibre direction of 400 mm were tested. Bending strength of structural timber was determined based on bending strength of small timber samples and correction factors which account for sample size, in accordance with EN 384 [45]. Bending strength of structural timber was determined as $f_{\mathrm{m,mean}} = 43.8$ N/mm^2, while mean value of timber modulus of elasticity parallel to wood fibre equalled to $E_{0,\mathrm{mean}} = 11242$ N/mm^2. Density of timber was determined in accordance with ISO 13061–2 [46]. A total of 40 samples with dimensions of $20 \times 20 \times 25$ mm were tested. Mean value of timber density was determined as $\rho_{\mathrm{mean}} = 424$ kg/m^3.

In addition, shear test parallel to wood fibre was performed according to ASTM D143-09 standard [47]. In accordance with these standards, the test was carried out on samples in a form of a notched cuboid so that the pressure is applied in the shear plane of a sample. A total of 20 samples were tested, which were cut so that the shear occurs in the longitudinal layer, along the tangential surface. Based on the test results, mean value of timber shear strength was determined as $f_{\mathrm{v,mean}} = 5.3$ N/mm^2.

Material properties were adopted based on the performed tests (exp) on small clear timber samples and values available in Gustafsson [48]. Due to the stress distribution effect in timber flexural members, tensile stress at failure is greater in bending than in axial tension. Hence, ultimate tensile stress was assumed to be equal to bending strength obtained in bending tests, which were conducted on small timber samples. The values are listed in Table 1.

The general relationships proposed by Bodig and Jayne [49] were used to calculate the moduli of elasticity in the radial and tangential direction, as well as shear moduli in the shear planes:

$$E_L : E_T : E_R \approx 20 : 1.6 : 1 \tag{8}$$

$$G_{LT} : G_{LR} : G_{TR} \approx 10 : 9.4 : 1 \tag{9}$$

$$E_L : G_{LT} \approx 14 : 1 \tag{10}$$

where E_{L}, E_{T} and E_{R} are the moduli of elasticity in the longitudinal, tangential and radial directions, respectively, while G_{LT}, G_{LR} and G_{TR} are the shear moduli in the shear orthotropic planes. The values of Poisson's rations ν_{LT}, ν_{LR} and ν_{TR} were adopted based on values given in [49] for softwood. The values of moduli of elasticity, shear moduli and Poisson's rations are given in Table 2.

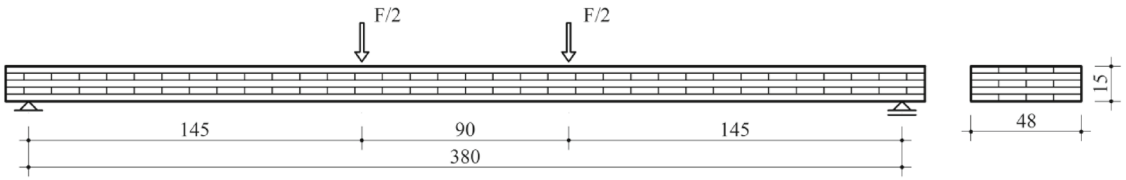

Fig. 5 Panel testing layout

Fig. 6 Test set-up for CLT specimens

3.2 Experimental test set-up for CLT specimens

The main experimental programme included testing of five CLT panels (specimens A1-A5), with dimensions: 48 cm width × 400 cm length × 15 cm thickness. The panels consisted of five 3-cm-thick layers made of boards (laminations) with approximate width of 12 cm. Longitudinal laminations were formed by joining the boards using finger joints. Arrangement of finger joints within the layer was arbitrary. Transverse boards did not contain finger joints due to their short lengths. In order to prevent deformations due to drying, longitudinal grooves were cut into the laminations. Melamine–urea–formaldehyde adhesive was used for finger joints and inter-layer bonding. Adjacent boards within the layers had no edge bonding.

All panels were tested in bending as simply supported beams with a span of 380 cm (approximately 25 times the panel thickness) symmetrically loaded with two concentrated forces at a distance of 90 cm (6 times the panel thickness), in accordance with EN 16351 [50]. With this arrangement of forces, a constant bending moment was obtained in the middle part of the panels, without shear force. A schematic illustration of the test layout is given in Fig. 5.

Experimental testing was performed in a closed steel frame (Fig. 6). The load was applied using a hydraulic jack. In the experimental procedure, the load was transformed from one concentrated force to two forces distributed along the panels' width using a steel rectangular hollow section with welded steel sheets at the points of force input. Steel roller bearings were used at the supports. Also, roller bearings were used at the load application points to ensure that the load acts vertically. Steel plates were placed under the load application points and at the supports to minimize local indentations.

The load was applied at a controlled rate of in order to achieve panel failure in about 5 min. Load application was measured using a loading cell. Deflection of the panels was measured using linear variable differential transducers (LVDTs). The mid-span deflection was measured on both sides using two LVDTs, positioned to allow reading near the neutral axis, while deflection at the supports was measured on both sides using four LVDTs. In addition to the measured deflections, in the mid-span, strains were measured around the cross section using strain gauges. Strain data from strain gauges, deflection data from LVDTs and corresponding load data from the loading cell were collected using the acquisition system.

During the testing of all panels, humidity and air temperature were controlled next to the testing frame. Humidity was between 50 and 60% and temperature was about 25 °C. Immediately after each test was completed, the moisture content of timber was measured using a digital hygrometer at various points on the panel. The recorded moisture content in all specimens ranged from 9.8 to 11.2%.

Table 3 Material elastic properties of a continuous lamina [MPa]

E_1	$E_2 = E_3$	$G_{12} = G_{13}$	G_{23}	ν_{12} (-)	ν_{13} (-)	ν_{23} (-)
11242	730.73	774.41	80.3	0.37	0.42	0.47

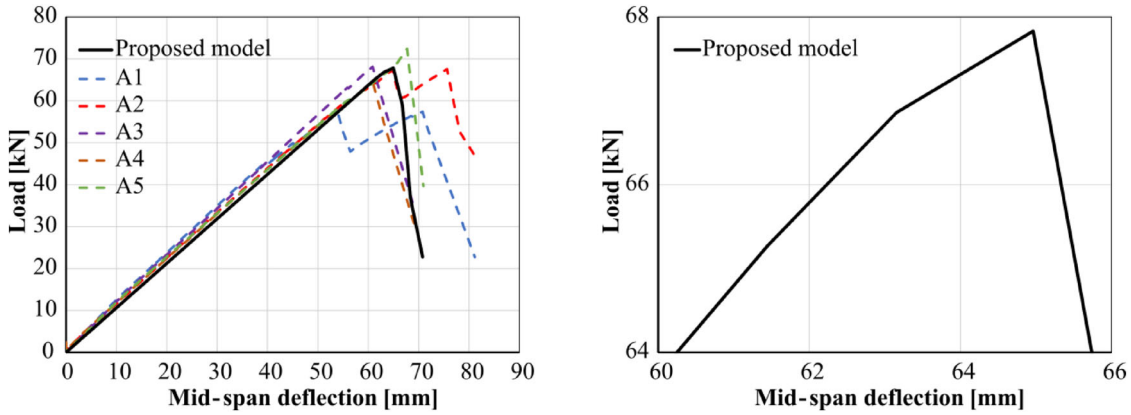

Fig. 7 Load–deflection curve predicted by the proposed model along with the load–deflection curves for all tested CLT panels (left); magnified load–displacement curve predicted using the proposed model (right)

3.3 Computational analysis and discussion

In the finite element model, geometry, boundary and loading conditions were adopted in accordance with the presented test set-up. Due to symmetry in loading and boundary conditions, only a quarter of the CLT panel was modelled to reduce the number of DOFs, with appropriate symmetry constraints: $V^{\mathrm{I}} = 0$ for the XZ symmetry plane and $U^{\mathrm{I}} = 0$ for the YZ one. The end support was modelled as a roller support, where the displacements in the thickness direction were constrained, while the displacements in longitudinal direction were allowed. Since the preliminary convergence study showed no considerable improvement in results for finer mesh, the computational stress analysis was performed using only 24×3 Q8 layered quadrilateral elements with reduced integration. Every lamina was divided into two sub-laminas, adopting the linear distribution of displacements along the sub-lamina thickness. In order to avoid stress concentrations, an external load was smeared on subarea of 160×240 mm^2, according to the experimental test set-up.

Table 3 provides the elastic properties of the lamina used in the computational analysis. The moduli for the 2 and 3 directions are the average values of the corresponding T and R values for solid timber, obtained experimentally, while the strength parameters are equal to those listed in Table 2. By including the characteristic element length into the material damage law, the model achieves constant dissipated fracture energy, regardless of the element dimensions, which minimizes the mesh dependency.

Figure 7, left, illustrates the load–deflection curve obtained using both the developed prediction model and experimental tests. Figure 7, right, shows a magnified curve from the computational analysis. In the experimental results, the displayed values of deflection at failure, for each specimen, represent the mean values of measurements of two LVDTs placed in the mid-span on both sides of the panel. A brittle behaviour of all experimentally tested CLT panels is observed, with a linear elastic behaviour until the load peak value is reached, followed by abrupt loss of stiffness leading to failure (dashed lines in Fig. 7, left). PFA conducted for CLT panel also showed linear elastic behaviour until failure, replicating experimental results very closely. It is barely seen (Fig. 7, right) that insignificant stiffness reduction occurs shortly before the peak value of the load is reached, when a single fibre start to buckle in the top longitudinal layer. Plasticization of timber in the compression zone is actually difficult to observe experimentally, due to early appearance of cracks in tension zone.

Failure of all experimentally tested specimens occurred due to a tensile failure of the outer longitudinal layer (FT failure), as shown in Fig. 8. Failure in tension zone is accompanied by pronounced shear cracks that extend along the glued line between outer longitudinal layer and adjacent transverse layer and/or through transverse layer. The cracks appear so close to the glueline since this is the weakest part of the lamella due to the cutting of fibres during sawing and discontinuity between the density and the moisture induced deformations between

Fig. 8 Typical failure mode of Series A panels (specimen A1)

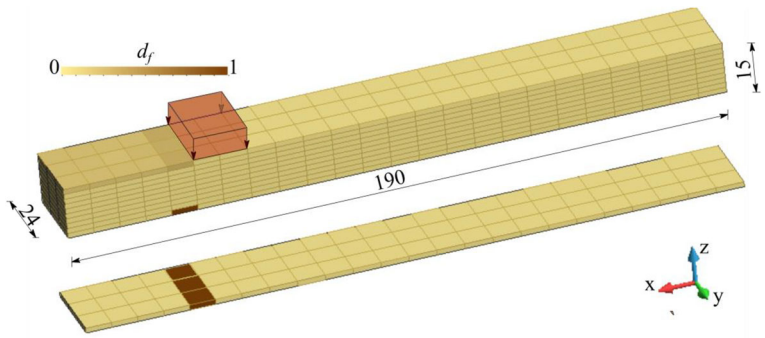

Fig. 9 Fibre failure patterns of CLT panel, plotted using the FLWTFEM at the failure load ($d_{ft} = 1$). The bottom figure illustrates only the bottom layer within a CLT panel

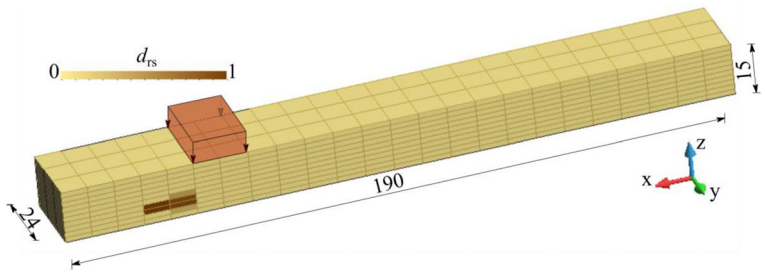

Fig. 10 Rolling shear (RS) failure pattern of CLT panel plotted using the FLWTFEM after the load reaches the maximum value and starts dropping

the adjacent boards (as indicated in [51]). In addition, a combination of fibre tearing and rolling shear failure was also observed. Tension failure was initiated at wood defects (knots) or finger joints of longitudinal lamina in maximum bending moment area, between load application points. At the moment of failure, simultaneous fracturing of several boards of the bottom longitudinal layer was observed in all specimens. The gradual post-peak decrease of the loads measured in experiments is a consequence of shear crack propagation both through the weakest part of the lamella in the vicinity of the glueline and the transverse layer.

The overall damage pattern predicted using the proposed model is illustrated through a spatial plots of fibre damage variables (Fig. 9) at the failure load, associated with the fibre tension ($d_{ft} = 1$). As can be seen from Fig. 9, ultimate failure occurred due to the FT failure of the bottom longitudinal lamina. This is quite similar to the observation from experiments (Fig. 8). At the moment of failure, plasticization of timber in the compression zone (see top longitudinal layer in Fig. 9) is barely noticeable. RS failure appears in transverse layer, after the load reaches the maximum value and starts dropping, as can be seen through spatial plots of transverse damage variables (Fig. 10). This is also in accordance with experimental observation.

Table 4 Results of experimental testing and computational analysis of considered CLT panels

Specimen	Maximum load F_{max} (kN)	Deflection at maximum load w_{odg} (mm)	Deflection at failure w_{max} (mm)	Bending stiffness EI_{global} (kNmm^2)	Failure mode
A1	57.8	53.8	71.4	12.26×10^8	FT
A2	67.5	75.6	75.6	11.49×10^8	FT
A3	68.1	60.9	60.9	11.92×10^8	FT
A4	64.2	60.8	60.8	11.24×10^8	FT
A5	72.4	67.7	67.7	11.44×10^8	FT
Average	66.0 (CV, 8.3%)	63.8 (CV, 12.9%)	67.3 (CV, 9.7%)	11.67×10^8 (CV, 3.5%)	/
Proposed model	67.83	64.96	64.96	11.2×10^8	FT
ARD (%)	2.77	1.81	3.48	4.03	/

CV coefficient of variation, *ARD* average relative differences

Both the experimental results and those from numerical simulations, in terms of maximum load and mid-span deflection at maximum load, mid-span deflection at ultimate failure and bending stiffness are given in Table 4. Corresponding values for loads–deflections were read from load–deflection curves (Fig. 7).

Average relative difference for the maximum load obtained using the proposed model against the experimental value is only 2.77%. When mid-span deflection at failure is concerned, numerical and experimental results were also compatible, with difference of 3.48%.

The out-of-plane bending stiffness of the panels was determined based on measurement of "global" deflection of the panels. "Global" deflection reflects a mechanism of both bending and shear deformation of CLT panels. Due to high span-to-depth ratio ($l/h \approx 25$) of tested panels which ensures the dominance of bending deformations, the influence of shear deformations on calculated bending stiffness can be neglected. Bending stiffness of tested panels was determined based on the slope of load–deflection curves, for the linear elastic region of behaviour between $0.1F_{max}$ and $0.4F_{max}$ (F_{max}—maximum load) according to the following expression:

$$EI_{global} = \frac{3 \cdot a \cdot l^2 - 4 \cdot a^3}{48 \cdot \left(\frac{w_2 - w_1}{F_2 - F_1}\right)} \tag{11}$$

where EI_{gobal} is the "global" bending stiffness; F_1 is the load corresponding to 10% of the maximum load ($0.1F_{max}$);F_2 is the load corresponding to 40% of the maximum load ($0.4F_{max}$); w_1 is the mid-span deflection corresponding to the loadF_1;w_1 is the mid-span deflection corresponding to the loadF_2; l is the spacing of specimen supports (span); and a is the distance of the applied force from the nearest support. Computational prediction of bending stiffness agreed well with experimental results, with a difference of 4.03%. These results confirm that timber can be effectively modelled as a homogeneous orthotropic material. The variability of elasticity modulus measurements was the reason for deviation between simulation and experimental results.

To get insight the deformation pattern within CLT specimens, an example of typical strain distribution for tested CLT panels at different load levels is given in Fig. 11, left. The profiles show compressive and tensile strains along x-axis as negative and positive values, respectively, and the position of strain gauges along the height on y-axis, measured from the lower edge of the cross section. The given strain values represent the mean values of the corresponding measurements on both sides of the specimen.

To evaluate the strain behaviour predicted using the proposed model, the longitudinal strain distribution through the thickness, at the mid-span of the CLT panel for different load levels, is illustrated in Fig. 11, right. Since these are plate elements composed of longitudinal and transverse layers in which there is no edge bonding of adjacent boards, a certain discrepancy in strain values measured on both sides of the panels was recorded. This is not the case for computationally obtained strain values due to the fact that each timber lamina was observed as a continuous layer.

Strain distribution in the cross section is linear up to failure, thus confirming the assumption of bending theory that plane sections remain plane during deformation. Measured strains on longitudinal and transverse laminas of the CLT panels indicate that there is no sliding between the laminas. This is in line with the perfect bonding assumption between laminas, used in the FLWT.

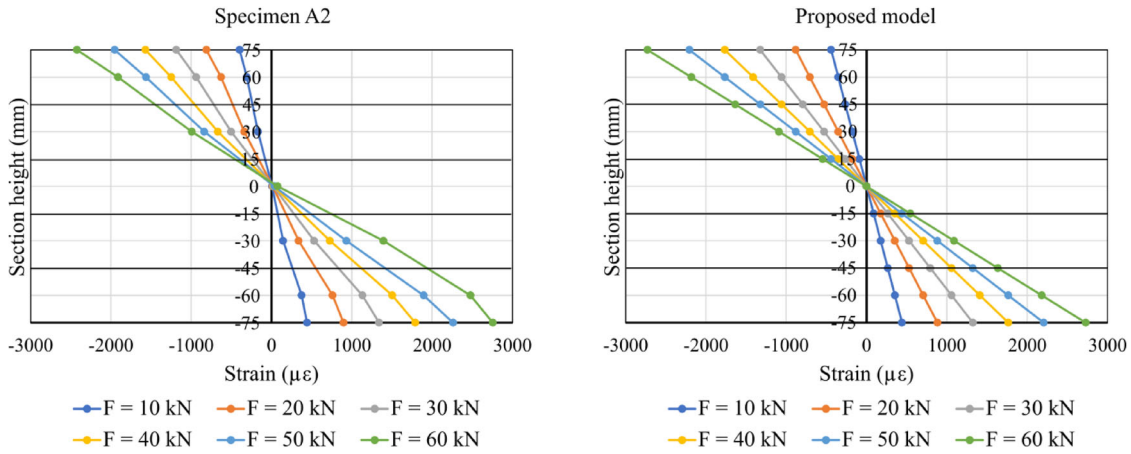

Fig. 11 Longitudinal strain distribution through the thickness, at the mid-span of CLT panel obtained from: left) experimental tests (specimen A2); right) proposed model

It can be verified that the overall strain distribution predicted by the proposed model is quite similar when compared against the experimental measured strains. Also, the strain values in tension and compression zones were approximately the same at all load levels. Small differences between numerical and experimental results can be justified due to the fact that each lamina was homogenized with the average modulus of elasticity, while in reality each lamina is inhomogeneous and the material properties of timber vary. With load increase, no displacement of neutral axis position was recorded, which confirms that wood plastification on the compressed side of the cross section was limited due to early appearance of cracks in tension zone.

4 Conclusions

In the paper, a reliable SCB-based computational model for progressive failure analysis of CLT panels under out-of-plane bending was developed. The model employs the layerwise kinematics, which provides the computationally efficient and accurate prediction of 3D stress and strain field on the lamina level within the CLT. This is a crucial prerequisite for prediction of damage initiation and progression in CLT. Damage initiation and failure modes on the lamina level are determined using the 3D Hashin failure criterion, while the post-failure behaviour of timber is described by distinct bilinear strain-softening curves to capture timber response in tension (brittle) and compression (ideally plastic), using the SCB approach.

Model validation is done through the extensive experimental testing programme on full-scale CLT specimens. In both the experiments and the computational simulations, the ultimate failure of the considered specimens occurred due the fibre tension failure scenario of the bottom longitudinal lamina. The rolling shear failure appeared in transverse layers, which was observed both in the experiments and FEM simulations.

Excellent agreement of predicted load–deflection curves and strain distributions verified that the proposed methodology can be efficiently applied in progressive failure analysis of mass timber (and other layered beam- and plate-like structures). The model is suitable for structural design of CLT structures in bending (with arbitrary geometry and boundary conditions), thus going beyond the classical analytical engineering tools for CLT design and analysis.

Acknowledgements This research was supported by the Science Fund of the Republic of Serbia, GRANT No. 7677448: Towards Sustainable Buildings: Novel Strategies for the Design of Vibration Resistant Cross-Laminated Timber Floors—Substrate4CLT. The financial support of the Ministry of Science, Technological Development and Innovation of the Republic of Serbia, through the project 200092, is also acknowledged.

Author contribution All authors contributed to the study conception and design. The first draft of the manuscript was written by E.J. and M.T. All authors commented on the first version of the manuscript, and the final version was written by I.G. and M.M. All authors read and approved the final manuscript. Experimental testing and data analysis were performed by I.G. and M.T. The computational model development and simulations were conducted by E.J. Necessary software modifications for the analyses were implemented by E.J. and M.M. Figures were generated by E.J. and M.T.

Funding Science Fund of the Republic of Serbia,7677448: Towards Sustainable Buildings: Novel Strategies for the Design of Vibration Resistant Cross-Laminated Timber Floors—Substrate4CLT, Ministry of Science, Technological Development and Innovation of the Republic of Serbia,200092.

Data availability No datasets were generated or analysed during the current study.

Declarations

Conflict of interests The authors declare no competing interests.

References

1. Jeleč, M., Varevac, D., Rajčić, V. (2018) Cross-laminated timber (CLT) – a state of the art report. Građevinar 70: 75–95. https://doi.org/10.14256/JCE.2071.2017
2. Brandner, R., Flatscher, D., Ringhofer, A., Schickhofer, G., Thiel, A.: Cross Laminated Timber (CLT): overview and development. Eur J Wood Wood Prod **74**(3), 331–351 (2016). https://doi.org/10.1007/s00107-015-0999-5
3. Communication from the Commission to the European Parliament, the European Council, the Council, the European Economic and Social Committee and the Committee of the regions - the European Green Deal. European Comission, Luxembourg, 2019.
4. Brandner, R., (2013) Production and technology of Cross Laminated Timber (CLT): State-of-the-art Report. Focus Solid Timber Solutions-European Conference on Cross Laminated Timber, Graz, Austria.
5. Stürzenbecher, R., Hofstetter, K., Eberhardsteiner, J., (2010) Cross Laminated Timber: a multi-layer, shear compliant plate and its mechanical behavior. In: 11th World Conference on Timber Engineering, Riva del Garda, Italy.
6. Franzoni, L., Lebée, A., Lyon, F., Foret, G.: Influence of orientation and number of layers on the elastic response and failure modes on CLT floors: modeling and parameter studies. Eur J Wood Wood Prod **74**(5), 671–684 (2016). https://doi.org/10.1007/s00107-016-1038-x
7. He, M., Sun, X., Li, Z., Feng, W.: Bending, shear, and compressive properties of three- and five-layer cross-laminated timber fabricated with black spruce. J. Wood Sci. **66**, 38 (2020). https://doi.org/10.1186/s10086-020-01886-z
8. Nie, X., (2015) Failure Mechanism of Rolling Shear Failure in Cross-Laminated Timber. PhD Thesis, The University of British Columbia, Vancouver, Canada.
9. Wang, Z., Zhou, J., Dong, W., Yao, Y., Gong, M.: Influence of technical characteristics on the rolling shear properties of cross laminated timber by modified planar shear tests. Maderas-Cienc Tecnol **20**, 469–478 (2018). https://doi.org/10.4067/S0718-221X2018005031601
10. Sciomenta, M., Di Egidio, A., Bedon, C., Fragiacomo, M.: Linear model to describe the working of a three layers CLT strip slab: Experimental and numerical validation. Adv. Struct. Eng. **24**(14), 3118–3132 (2021). https://doi.org/10.1177/13694332211020403
11. Mestek, P., Kreuzinger, H., Winter, S., (2011) Design Concept for CLT - reinforced with Self-Tapping Screws. In: 44th CIB-W18 Meeting, Alghero, Italy.
12. Zhou, Q., Gong, M., Chui, Y.H., Mohammad, M.: Measurement of rolling shear modulus and strength of cross laminated timber fabricated with black spruce. Constr Build Mat **64**, 379–386 (2014). https://doi.org/10.1016/j.conbuildmat.2014.04.039
13. Hochreiner, G., Fussl, J., Eberhardsteiner, J.: Cross Laminated Timber plates subjected to concentrated loading. Strain **50**(1), 68–71 (2013). https://doi.org/10.1111/str.12068
14. Hochreiner, G., Fussl, J., Serrano, E., Eberhardsteiner, J.: Influence of wooden board strength class on the performance of Cross Laminated Timber plates investigated by means of full-field deformations measurements. Strain **50**(2), 161–173 (2014). https://doi.org/10.1111/str.12077
15. Pagano, N.: Exact solutions for rectangular bidirectional composites and sandwich plates. J. Compos. Mater. **4**, 20–34 (1969). https://doi.org/10.1177/002199837000400102
16. Pagano, N.: Influence of shear coupling in cylindrical bending of anisotropic laminates. J. Compos. Mater. **4**, 330–343 (1970). https://doi.org/10.1177/002199837000400305
17. van der Put , T. (1982) A general failure criterion for wood. In: 15th Conseil Industriel des Bois-International Union of Forestry Research Organizations Meeting, Boras, Sweden
18. Albostami, A.S., Wu, Z., Cunningham, L.S.: Assessment of cross-laminated timber panels by the state-space approach. Adv. Struct. Eng. **22**(11), 2375–2391 (2019). https://doi.org/10.1177/1369433219841504
19. Navaratnam, S., Ngo, T., Christopher, P., Linforth, S.: The use of digital image correlation for identifying failure characteristics of cross-laminated timber under transverse loading. Measurement **154**, 107502 (2020). https://doi.org/10.1016/j.measurement.2020.107502
20. Huang, Z., Huang, D., Chui, Y.H., Shen, Y., Daneshvar, H., Sheng, B., Chen, Z.: Modeling of cross-laminated timber (CLT) panels loaded with combined out-of-plane bending and compression. Eng. Struct. **250**, 113335 (2022). https://doi.org/10.1016/j.engstruct.2021.113335
21. Cherry, R., Manalo, A., Karunasena, W., Stringer, G.: Out-of-grade saw pine: A state-of-the-art review on challenges and new opportunities in cross laminated timber (CLT). Constr Build Mat **211**, 858–868 (2019). https://doi.org/10.1016/j.conbuildmat.2019.03.293
22. ANSI/APA PRG 320 (2019) Standard for performance related cross-laminated-timber
23. CSA O86–14 (R2019) Engineering design in wood

24. Daneshvar, H., Niederwestberg, J., Dickof, C., Chui, Y.H.: Structural behaviour of deep CLT lintels subjected to concentric and eccentric loading. J. Build. Eng. **43**, 103101 (2021). https://doi.org/10.1016/j.jobe.2021.103101
25. EN 1995:2008 (2008) Eurocode 5: Design of timber structures—Part 1–1: General-Common rules and rules for buildings
26. Qiu, L.P., Zhu, E.C., van de Kuilen, J.W.G.: Modeling crack propagation in wood by extended finite element method. Eur J Wood Wood Prod **72**, 273–283 (2014). https://doi.org/10.1007/s00107-013-0773-5
27. Ma, Y., Wang, X., Begel, M., Dai, Q., Dickinson, Y., Xie, X., Ross, R.J.: Flexural and shear performance of CLT panels made from salvaged beetle-killed white spruce. Constr Build Mat **302**, 124381 (2021). https://doi.org/10.1016/j.conbuildmat.2021.124381
28. Williams, K.V., Vaziri, R., Poursartip, A.: A physically based continuum damage mechanics model for thin laminated composite structures. Int. J. Solids Struct. **40**(9), 2267–2300 (2003). https://doi.org/10.1016/S0020-7683(03)00016-7
29. Forghani, A., Zobeiry, N., Poursartip, A., Vaziri, R.: A structural modelling framework for prediction of damage development and failure of composite laminates. J Compos Mat **47**(20–21), 2553–2573 (2013). https://doi.org/10.1177/0021998312474044
30. Forghani, A., Poursartip, A., Vaziri, R.: An orthotropic non-local approach to modeling intra-laminar damage progression in laminated composites. Int. J. Solids Struct. **180**, 160–175 (2019). https://doi.org/10.1016/j.ijsolstr.2019.07.015
31. Reiner, J., Feser, T., Schueler, D., Waimer, M., Vaziri, R.: Comparison of two progressive damage models for studying the notched behavior of composite laminates under tension. Compos. Struct. **207**, 385–396 (2019). https://doi.org/10.1016/j.compstruct.2018.09.033
32. Nagaraj, M.H., Reiner, J., Vaziri, R., Carrera, E., Petrolo, M.: Progressive damage analysis of composite structures using higher-order layer-wise elements. Compos Part B-Eng **190**, 107921 (2020). https://doi.org/10.1016/j.compositesb.2020.107921
33. Bažant, Z.P.: Instability, ductility, and size effect in strain-softening concrete. J. Eng. Mech. **102**(2), 331–344 (1976). https://doi.org/10.1061/JMCEA3.0002111
34. Ibrahimbegović, A.: Nonlinear Solid Mechanics. Springer, Netherlands, Dordrecht, Netherlands (2009)
35. Lavrenčič, M., Brank, B.: Failure analysis of ribbed cross-laminated timber plates. Coupl. Syst. Mech. **7**(1), 79–93 (2018)
36. Reddy, J.N.: Mechanics of laminated composite plates and shells: theory and analysis. CRC Press, Boca Raton, Florida (2004)
37. Hashin, Z.: Failure criteria for unidirectional fibre composites. J. Appl. Mech. **47**, 329–334 (1980). https://doi.org/10.1115/1.3153664
38. Jočić, E., Marjanović, M.: Progressive failure analysis of open-hole composite laminates using FLWT-SCB prediction model. Int. J. Mech. Sci. **227**, 107407 (2022). https://doi.org/10.1016/j.ijmecsci.2022.107407
39. Marjanovic, M., Meschke, G., Damnjanovic, E.: Object-oriented framework for 3D bending and free vibration analysis of multilayer plates: Application to cross-laminated timber and soft-core sandwich panels. Compos. Struct. **255**, 112–159 (2021). https://doi.org/10.1016/j.compstruct.2020.112859
40. Dourado, N., Morel, S., de Moura, M.F.S.F., Valentin, G., Morais, J.: Comparison of fracture properties of two wood species through cohesive crack simulations. Compos Part A-Appl S **39**, 415–427 (2008). https://doi.org/10.1016/j.compositesa.2007.08.025
41. Marjanovic, M., Markovic, N., Damnjanovic, E., Cvetkovic, R.: Three-dimensional stress analysis and design of cross-laminated timber panels using full-layerwise-theory-based finite element method. Thin Wall Struct **157**, 107–156 (2020). https://doi.org/10.1016/j.tws.2020.107156
42. GiD Customization Manual (2016) CIMNE - International Center for Numerical Methods in Engineering.
43. EN 338:2009 (2009) Structural timber - Strength classes
44. EN 408:2010+A1:2012 (2012) Timber structures - Structural timber and glued laminated timber - Determination of some physical and mechanical properties
45. EN 384:2016 (2016) Structural timber - Determination of characteristic values of mechanical properties and density
46. ISO 13061–2:2014 (2014) Physical and mechanical properties of wood - Test methods for small clear wood specimens—Part 2: Determination of density for physical and mechanical tests
47. ASTM D143–09 (2009) Standard test methods for small clear specimens of timber
48. Gustafsson, J.: Fracture Perpendicular to Grain—Structural Applications. In: Engineering, T. (ed.) Thelandersson S and Jörgen Larsen H). John Wiley & Sons Inc (2003)
49. Bodig, J., Jayne, B.A.: Mechanics of wood and wood composites. Van Nostrand Reinhold, New York (1982)
50. EN 16351:2021 (2021) Timber structures—Cross laminated timber—Requirements
51. Dietsch, P., Tannert, T.: Assessing the integrity of glued-laminated timber elements. Constr. Build. Mat. **101**(2), 1259–1270 (2015). https://doi.org/10.1016/j.conbuildmat.2015.06.064)